Journal of Photochemistry & Photobiology, B: Biology 235 (2022) 112543

Contents lists available at ScienceDirect

Journal of Photochemistry & Photobiology, B: Biology

journal homepage: www.elsevier.com/locate/jphotobiol

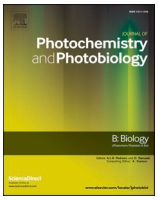

Photodynamic inactivation of *Staphylococcus aureus* in the presence of aggregation-prone photosensitizers based on BODIPY used at submicromolar concentrations

Diego Navarro-Barreda [a], Rosa de Llanos [b], Juan F. Miravet [a], Francisco Galindo [a,*]

[a] Departamento de Química Inorgánica y Orgánica, Universitat Jaume I, Avda. Sos Baynat s/n, 12071 Castellón, Spain
[b] Unidad Predepartamental de Medicina, Universitat Jaume I, Avda. Sos Baynat s/n, 12071 Castellón, Spain

ARTICLE INFO

Keywords:
Photodynamic inactivation
Photo-antimicrobials
Singlet oxygen
Photosensitizers
S. aureus
E. coli
ESKAPE

ABSTRACT

Two new brominated BODIPYs (**1** and **2**) bearing amino acid-based chains (L-valine for **1**, and dimethyl-L-lysine for **2**) were synthesized and characterized. In organic solvents, **1** and **2** were fully soluble and showed the photophysical properties expected for brominated BODIPY dyes, including efficient generation of singlet oxygen ($^1O_2$), upon irradiation. In contrast, in aqueous media, both compounds were prone to aggregation and the photo-induced generation of $^1O_2$ was halted. Despite the lack of generation of this reactive species in aqueous media (*in cuvette*), both **1** and **2** have positive antimicrobial Photodynamic Inactivation (aPDI) effect. The activity against gram-positive *Staphylococcus aureus* and gram-negative *Escherichia coli* was determined through the inactivation curves, with a total energy dose of 5.3 J/cm^2 (white light LED used as an energy source). Compound **2** was highly active against both gram-positive and gram-negative bacteria (3 log CFU/mL reduction was obtained at 0.16 μM for *S. aureus* and 2.5–5.0 μM for *E. coli*), whereas **1** was less effective to kill *S. aureus* (3 log CFU/mL at 0.32 μM) and ineffective for *E. coli*. The higher efficiency of **2**, as compared to **1**, to reduce the population of bacteria, can reside in the presence of a protonatable residue in **2**, allowing a more effective interaction of this molecule with the cell walls of the microorganisms. In order to explain the lack of reactivity in pure aqueous media (*in cuvette*) and the contrasting good activity in the presence of bacterial cells it can be hypothesized that upon interaction with the walls of the microorganisms, the aggregated photosensitizers suffer a disaggregation process restoring the ability to generate $^1O_2$, and hence leading to efficient photodynamic activity against these pathogenic microorganisms, in agreement with the similar effect observed recently for porphyrinoid photosensitizers.

1. Introduction

Antimicrobial resistance (AMR) has been increasing steadily during the last decades and today is one of the most important threats identified by the World Health Organization (WHO). This problem is particularly serious in health settings where the contagion by antibiotic-resistant microorganisms causing nosocomial infections is commonplace [1]. Although the development of new drugs with antibiotic properties is stacked for many reasons [2], alternative ways to stop the spreading of pathogenic microorganisms have been developed in recent years. One of them is the antimicrobial Photodynamic Inactivation (aPDI), which employs photosensitizing agents (dyes) capable of absorbing light photons promoting them to an excited state. The excess energy absorbed by photosensitizers can be transferred to the surrounding oxygen, leading to reactive oxygen species (ROS) having a cytotoxic effect on the nearby microorganisms. Most studied photoantimicrobial systems are based on the so-called type II photosensitizing process, in which the generated ROS is singlet oxygen ($^1O_2$). Other ROS include superoxide anion ($O_2^{\bullet-}$) and hydroxyl radical (HO•) [3]. Recently, aPDI has been also proposed as a complementary way to eliminate the SARS-CoV-2 virus [4]. Details about the process of photosensitization and the nature and effects of the generated ROS species have been described in the literature [5–14].

Regarding photosensitizers, the vast majority of systems developed and studied so far consist of water-soluble molecules belonging to different chemical families like xanthene and phenothiazinium dyes, porphyrins and phthalocyanines, fullerene derivatives, and others

* Corresponding author.
E-mail address: francisco.galindo@uji.es (F. Galindo).

https://doi.org/10.1016/j.jphotobiol.2022.112543
Received 26 March 2022; Received in revised form 29 July 2022; Accepted 8 August 2022
Available online 10 August 2022

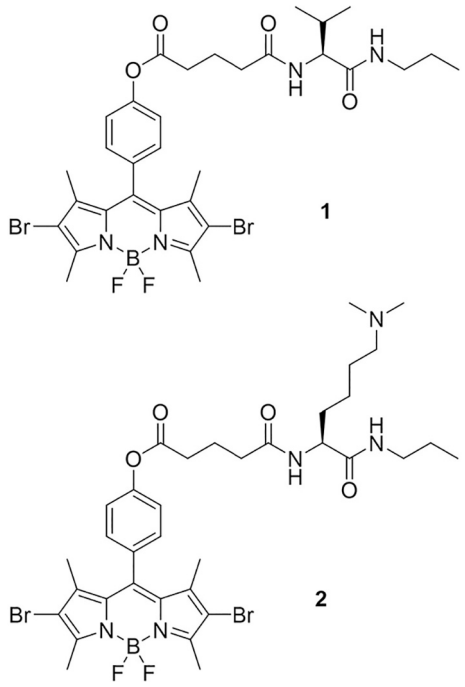

Fig. 1. Synthetic BODIPY-based photosensitizers (**1** and **2**) studied in this work.

[15,16]. To complete the picture, in recent times a new field has emerged from the realm of soluble photosensitizers and the development of polymeric photoactive materials with photoantimicrobial properties is attracting increasing attention. These novel materials have been developed to prevent contagion rather than for therapeutic use [17–23]. But, the therapeutic action against a certain infection requires the development of approaches using either soluble molecules or colloidal formulations with diffusion capabilities, so that the photosensitizer reaches the microbial cell and attains close interaction with the pathogen since the lifetime of cytotoxic $^1O_2$ is extremely short and allows only a limited radius of action after its generation [24]. One interesting strategy developed in recent times has been the incorporation of photosensitizers on nanostructures, acting as carriers, with the purpose of delivery to specific cellular targets [25,26]. A more straightforward approach has been the design of photosensitizers with self-assembling properties. In this case, the formed nanostructures are typically unable to generate $^1O_2$ upon irradiation, due to quenching of the excited states by π-π stacking, but upon interaction with a disassembling input, like proteins in the outer membrane of the microbe, restoration of the ability to generate cytotoxic ROS occurs, triggering the therapeutic action. The main advantage of this strategy is that a high local concentration of photosensitizer can be delivered to a single cell since the nanoparticles are formed exclusively by the photoactive molecule. This approach has been recently demonstrated for phthalocyanines, showing antimicrobial [27,28] and anticancer [29–31] properties. A very recent review collects a series of papers reporting this "one-for-all" approach in which the photoactive drug is at the same time the carrier and the cargo, avoiding the use of complex nano-delivery systems [32].

The nanosystems above described are all based on photosensitizers of the porphyrinoid family. However, one drawback of this class of photosensitizers is the complexities of their syntheses and the use of cumbersome purification procedures to obtain well-characterized stocks. Among the new photosensitizers object of attention, derivatives of 4,4-difluoro-bora-3a,4a-diaza-*s*-indacene (BODIPY) have been gaining importance as agents with photoantimicrobial and photoanticancer effects. This class of dyes have much more friendly synthetic routes and less problematic purification sequences [33–36]. Providing the proven advantages of the "one-for-all" approach above described, it would be interesting to know whether the same strategy could be adapted to BODIPY-based photosensitizers. For such reason, we envisaged that a BODIPY-based photosensitizer properly functionalized with an architecture prone to self-assembly would lead to nanoparticles with foreseeably relevant antibacterial properties upon disassembly. To the best of our knowledge, although some BODIPY dyes have been described (especially in recent years) [37–43] against pathogenic microorganisms, no example of assembly/disassembly of a BODIPY photosensitizer has been described in the context of aPDI. Here we describe two examples of BODIPY dyes (**1** and **2** in Fig. 1) showing such behaviour, leading to a remarkable photodynamic antimicrobial activity on both gram-positive (*Staphylococcus aureus*) and gram-negative (*Escherichia coli*) bacteria. Specifically, **2** proved to be a successful photoantimicrobial agent against *S. aureus,* causing a disinfection effect (99.9% reduction of the bacterial population or 3 log CFU/mL) at a concentration of only 0.16 μM.

2. Materials and Methods

2.1. Materials

Commercially available reagents and HPLC grade solvents were purchased from commercial suppliers and used without further purification. Reactions that required an inert atmosphere were carried out under N_2. NMR spectra were recorded on a Bruker Advance III HD spectrometer (400 MHz for ^{1}H NMR, 101 MHz for ^{13}C NMR) in the indicated solvent at 30 °C. All chemical shifts (δ) are quoted in parts per million (ppm) downfield from tetramethylsilane (TMS) and coupling constants (J) are quoted in Hertz (Hz). Mass spectra were recorded at a Mass Spectrometry triple Quadrupole Q-TOF Premier (Waters) apparatus with simultaneous Electrospray and APCI probe. The photophysical properties were measured with a JASCO FP-8300 fluorometer and a JASCO V-630 UV–Vis spectrophotometer. Lifetime measurements were performed by the time-correlated single-photon counting (TCSPC) technique using an IBH-5000 U instrument. The excitation source was a 464 nm nanoLED (1.4 ns pulse width), and data fitting was done using the IBH DAS6 fluorescence decay analysis software via the monoexponential eq. ($I(t) = I_0 \exp.(-t/\tau)$). The size distribution of nanoparticle measurements was recorded using a Zetasizer Nano-ZS90 (Malvern Instruments). Automatic optimization of beam focusing and attenuation was applied for each sample.

2.2. Synthesis

All the synthetic procedures are described in the Electronic Supporting Information (ESI) file.

2.3. Determination of Fluorescence Quantum Yields

Samples were measured using 3 mL (10 mm path length) quartz cuvettes. For fluorescence quantum yield determination, Rhodamine 6G was used as a standard ($\Phi_f = 0.94$ in ethanol, $\lambda_{ex} = 488$ nm). The concentrations of BODIPYs and standard were adjusted so that the absorbance was equal at the excitation wavelength (488 nm). The quantum yields of **1** and **2** were calculated from the following equation:

$$\Phi_f^i = \frac{F^i n_i^2}{F^s n_s^2}\Phi_f^s$$

where Φ_f refers to the quantum yields; F are the integrated intensities (areas under the curve) of the emission spectra, and n denotes the refractive indexes. The subscripts s and i refer to the standard and the sample, respectively. The fluorescence spectra were recorded in the wavelength range of 495–750 nm.

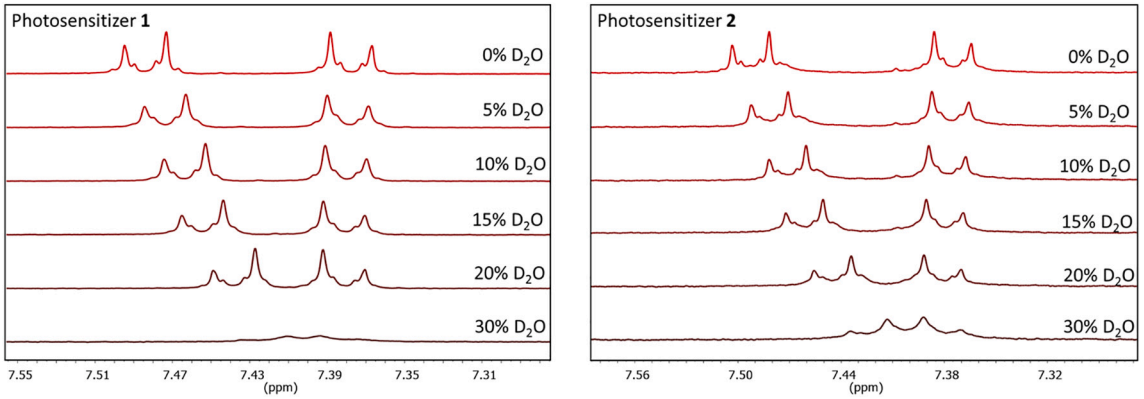

Fig. 2. Partial ^{1}H NMR spectra (400 MHz, 298 K) of **1** (top) and **2** (bottom), both 2 mM, in DMSO-d_6:D_2O mixtures.

2.4. Photochemical Generation of Singlet Oxygen ($^1O_2$)

The ability of **1** and **2** to generate singlet oxygen ($^1O_2$) was estimated using 9,10-dimethylanthracene (DMA) and the analogous water-soluble trap 9,10-anthracenediyl-bis(methylene)-dimalonic acid (ABDA). Photooxygenation reactions were conducted inside a quartz cuvette containing aerated solutions of DMA or ABDA (50 μM) and the photosensitizer (with an absorbance of 0.07 at 525 nm) in the corresponding solvent (acetonitrile, acetonitrile:PBS 6:4, PBS). Samples were irradiated using a light-emitting diode (LED) lamp (11 W, ca. 400–700 nm; 117 mW/cm^2) at timed intervals. The photooxygenation reaction was monitored following the decrease of the absorbance at 377 and 379 nm for DMA and ABDA, respectively, in a JASCO V-630 UV–Vis spectrophotometer. The kinetic traces were fitted to a pseudo-first-order kinetic model.

2.5. Quantum Yields Determination for Singlet Oxygen Generation (Φ_Δ)

Singlet oxygen generation quantum yields were determined using a direct measurement of near-infrared luminescence at 1275 nm. Steady state-photoluminescence (PL) measurements were conducted through a photoluminescence spectrophotometer (Fluorolog 3–11, Horiba). An excitation wavelength of 532 nm was used to perform the PL measurements. The singlet oxygen measurements were carried out in acetonitrile at absorbances of 0.3 at the excitation wavelength. Rose Bengal (RB) in acetonitrile ($\Phi_\Delta = 0.71$) was used as a standard [44]. Φ_Δ values were calculated using the following equation:

$$\Phi_\Delta^b = \frac{\Phi_\Delta^a}{I^a} I^b$$

where Φ_Δ^a is the quantum yield of RB and I^a and I^b are the integrated phosphorescence emission intensities of $^1O_2$ at 1275 nm for Rose Bengal and BODIPY derivatives, respectively.

2.6. Antibacterial Photodynamic Assays

E. coli ATCC 25922 and *S. aureus* ATCC 29213 were used as model microorganisms. Bacterial cultures were prepared from a pure culture of the chosen microorganism using the streak plate method and incubated aerobically on Mueller Hinton Agar (MHA) at 37 °C for 24 h. Colonies were suspended in sterile water solution to achieve a McFarland 1.0 density and diluted 200-fold (approx. 1.5 × 10^6 cells/mL). Stock solutions (1 mM) of **1** and **2** in dimethyl sulfoxide (DMSO) were subsequently diluted with a DMF:H_2O (1:1) mixture to obtain the desired concentrations (final concentrations of DMSO and DMF were less than 1% and 2%, respectively). Aliquots (10 μL) of each concentration of photosensitizers (final concentration of the photosensitizers ranged from 0.08 to 10 μM) and aliquots of each cell inocula (190 μL) were placed into a 96-well plate. Cell suspensions were immediately irradiated, without any dark incubation period (white light from a LED Flood Light 50 W, total energy dose 5.3 J/cm^2 after 60 s of irradiation, orbital shaking at 120 rpm). One plate from each experiment was not irradiated and served as a control (dark control). Light-alone controls (without photosensitizer) were also performed.

Relative cell survival for both irradiated and dark conditions was evaluated by counting colony-forming units (CFU) on MHA. To do so, each sample from each 96-well plate was serially diluted 10-fold in sterile distilled water. Drops (5 μL) of each dilution and the original suspension were spotted onto MHA plates and incubated at 37 °C for 24 h. Each experiment was performed in duplicate on three independent occasions. The results are expressed as mean ± standard deviation.

2.7. Confocal Laser Scanning Microscopy (CLSM)

S. aureus and *E. coli* suspensions (McFarland 1.0, approx. 10^8 cells/mL) were prepared similarly as stated above, but bacteria (190 μL) and photosensitizers (10 μL) were brought into contact using cell culture imaging dishes instead (μ-Slide 4 Well, Ibidi, GmbH, Martinsried, Germany). Cells were treated with compounds **1** and **2** at 10 μM. CLSM images were measured 15 min after bringing by using an inverted confocal microscope Leica TCS SP8 with an HC PL APO CS2 63×/1.40 oil immersion objective. The excitation wavelength was set at 514 nm (argon ion laser) and the emission was recorded from 520 to 650 nm. The measurements were carried out in PBS, pH 7.4.

Application of the propidium iodide (PI) protocol: samples were prepared in the same manner and after finishing irradiation (white light, 5.3 J/cm^2, 60 s, orbital shaking at 120 rpm), the samples were stained with PI for 15 min at room temperature and the bacterial viability was assessed. The excitation wavelength was set at 561 nm and the fluorescent emission was recorded from 650 to 700 nm. CLSM images were obtained on the same confocal microscope as before.

3. Results and Discussion

Compounds **1** and **2** were designed taking into account two considerations. First, a BODIPY structure carrying bromide atoms was selected, since it is well-known that the population of the excited triplet state is enhanced due to the presence of this heavy element [33]. Second, in previous studies from our research group, we have described a series of molecular structural motifs (typically alkyl chains and amino acid derivatives), leading to efficient self-association to give structures like fibres or aggregated particles of nanometric size [45–49]. The nature of the amino acid used as a building block determines greatly the propensity to aggregation. Combining these two ideas, compounds **1** and **2** were designed, synthesized and characterized using ^{1}H/^{13}C Nuclear Magnetic Resonance (NMR) and High-Resolution Mass Spectrometry

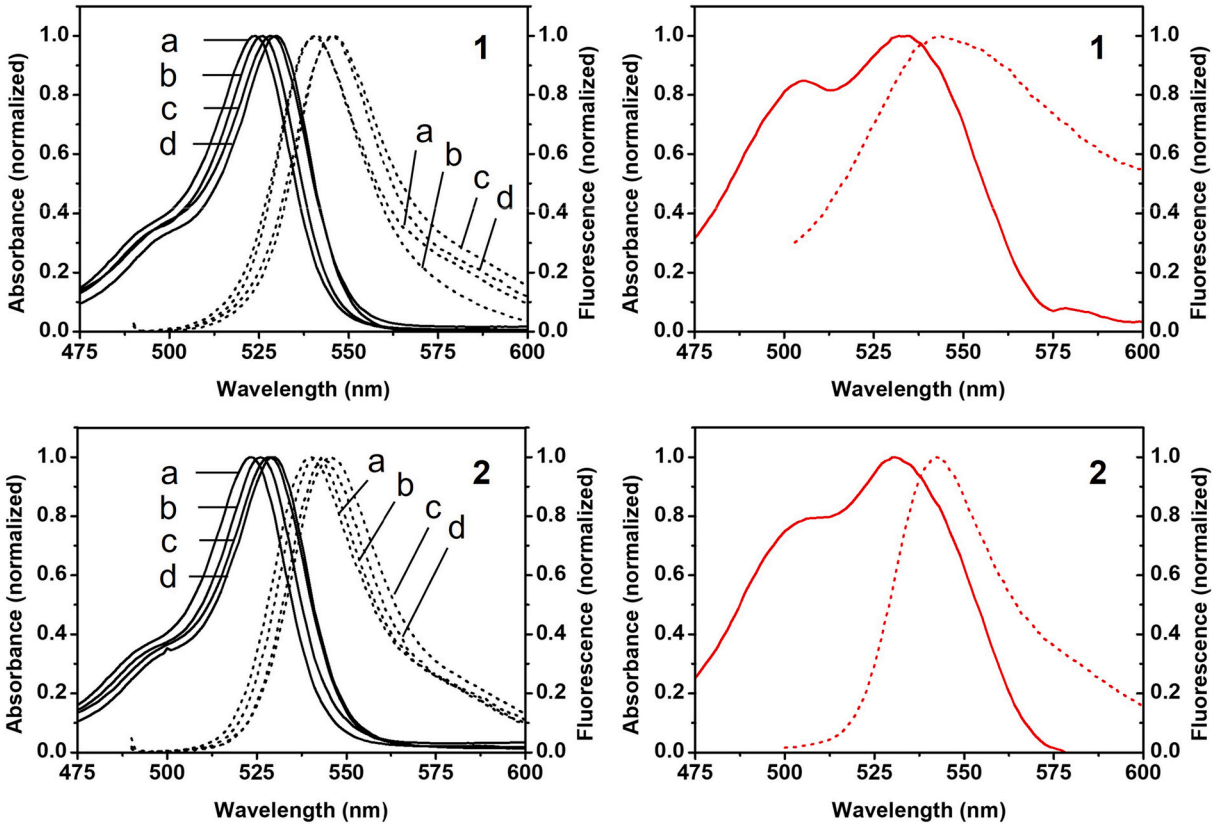

Fig. 3. Left: Normalized absorption (solid line) and emission spectra (dashed line, λ_{ex} = 485 nm) of **1** and **2** (5 μM) in (a) acetonitrile, (b) ethanol (c) DMSO and (d) dichloromethane; Right: absorption (solid line) and emission (dashed line, λ_{ex} = 485 nm) of **1** and **2** in aqueous solution (PBS, pH 7.4).

Table 1
Overview of the photophysical properties of the studied BODIPY dyes measured in different solvents.

Compound	Solvent	λ_{abs} [nm]	λ_{em} [nm]	Δλ [nm]	ϕ_F[a]	τ_F [ns][b]	k_r[c]	k_{nr}[c]	ϕ_Δ[d]
1	ACN	524	540	16	0.10	1.4	0.07	0.64	0.89
	DCM	530	545	15	0.28	1.7	0.16	0.42	ND
	EtOH	526	541	15	0.25	ND	ND	ND	ND
	DMSO	528	546	18	ND	ND	ND	ND	ND
2	ACN	523	540	17	0.15	1.3	0.11	0.65	0.66
	DCM	530	543	13	0.28	1.7	0.16	0.42	ND
	EtOH	526	541	15	0.19	ND	ND	ND	ND
	DMSO	528	545	17	ND	ND	ND	ND	ND

Abbreviation: ND; not determined.
[a] Using Rhodamine 6G as a standard in ethanol (0.94, λ_{ex} = 488 nm).
[b] Mono exponential fit, $I(t) = I_0 \exp.(-t/\tau)$.
[c] $k_r = \phi_F/\tau_F$ and $k_{nr} = (1 - \phi_F)/\tau_F$.
[d] Using Rose Bengal as a standard in acetonitrile (Φ_Δ = 0.71, λ_{ex} = 532 nm).

(HRMS). Synthetic details and the basic characterization data can be found in the Electronic Supporting Information (ESI) file (**Scheme S1** and **Fig. S1-S4)**. It must be noted that **1** derives from valine and **2** from lysine. The goals of this research are (a) to determine the influence of the amino acid building block on the aggregation and photochemical activity, and (b) to test the ability of **1** and **2** to act as photosensitizing agents for aPDI.

Compounds **1** and **2** tend to form aggregates in aqueous media as demonstrated by ^{1}H NMR measurements in mixtures of DMSO-d_6 and D_2O. As can be seen in Fig. 2, solutions of **1** or **2** in 100% DMSO-d_6 yield well-resolved spectra (aromatic protons shown) but upon increasing the proportion of D_2O the intensity of the peaks is reduced progressively till almost complete fading for a mixture containing 70% DMSO-d_6. As it has been shown previously, the formation of supramolecular assemblies implies the disappearance of signals from the spectrum [50]. Moreover, comparing **1** and **2** it can be deduced that valine derivative **1** is more prone to self-assembly than lysine-derived **2** since signals of the former have a much lower intensity than the ones of the latter (see **Fig. S5**). These observations were corroborated by Transmission Electron Microscopy (TEM) and Dynamic Light Scattering (DLS) as it can be seen in **Fig. S6**. DLS studies afforded average particle sizes of 370 nm (PdI = 0.51) and 180 nm (PdI = 0.16) for **1** and **2**, respectively.

The photophysical properties of **1** and **2** were studied using fluorescence (steady-state and time-resolved) and UV–Vis absorption spectroscopies. The absorption and emission features of **1** and **2** in organic solvents (acetonitrile, ethanol, DMSO and dichloromethane) coincide with those described in the literature for similar BODIPY dyes (see Fig. 3 and **Fig. S8-S9**), i.e., absorptions in the range ca.450–550 nm and emissions in the range ca. 500–600 nm, with low fluorescence quantum yields (ϕ_F, ca. 0.1–0.3) and short emission lifetimes (τ_F, ca. 1.3–1.7 ns)

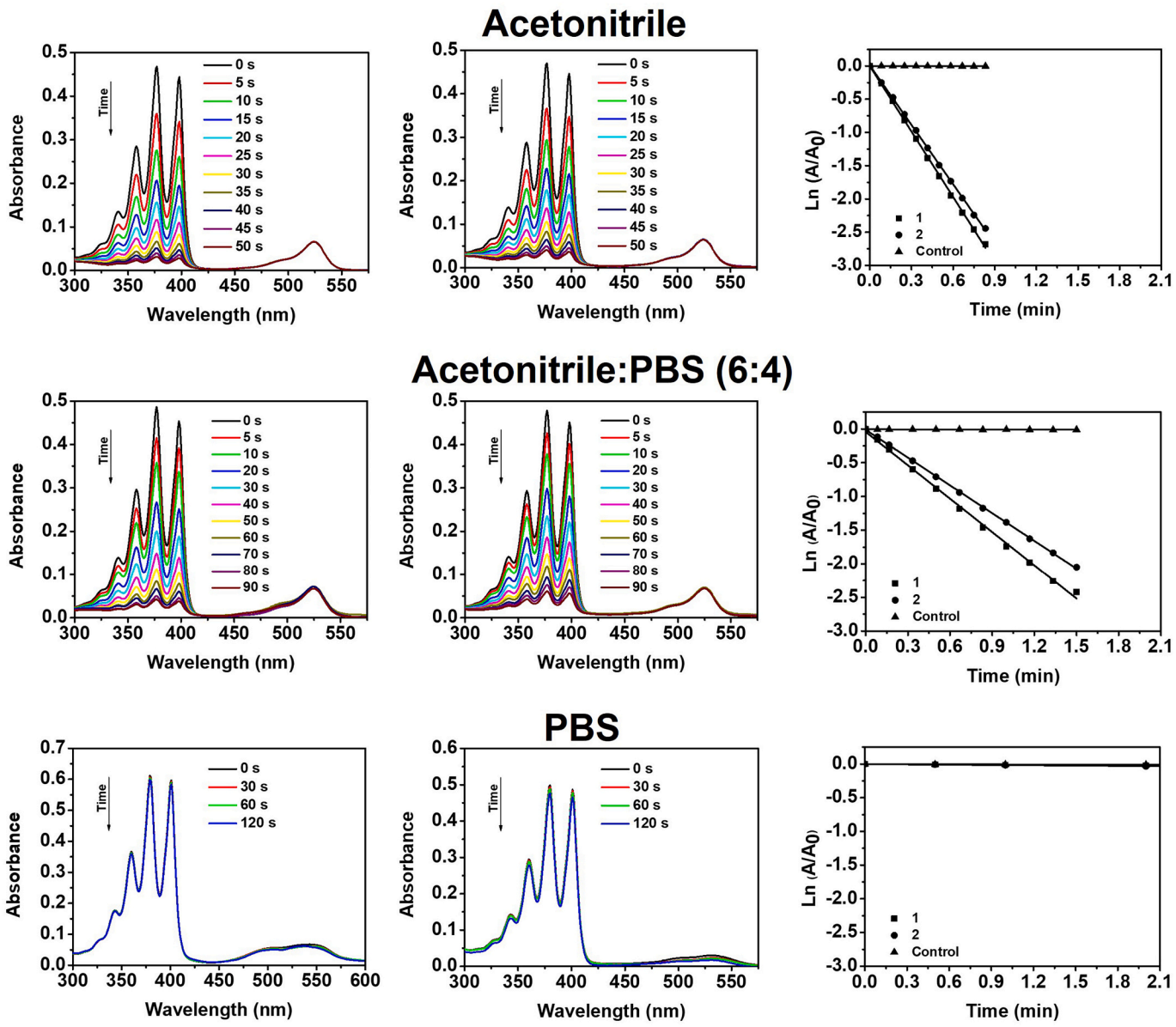

Fig. 4. Evaluation of the singlet oxygen generation ability of **1** and **2**. Left and central columns: UV–Vis spectra monitoring the photooxidation kinetics of DMA (for acetonitrile and acetonitrile:PBS) or ABDA (for PBS) by $^1O_2$ employing **1** (left) and **2** (center) as a photosensitizers. Right column: kinetic analysis using the absorbances of DMA or ABDA (at 377 and 379 nm, respectively) as a function of the irradiation time (for both **1** and **2** and also control without photosensitizer).

[33]. The specific data for each compound can be found in Table 1 along with the calculated radiative and non-radiative decay constants. The ability to generate $^1O_2$ was estimated by measuring the corresponding quantum yield of generation of this species (ϕ_Δ) in acetonitrile using the phosphorescence emission of $^1O_2$ at 1275 nm (**Fig. S10**). Compound **1** proved to be more efficient in generating ROS, with a (ϕ_Δ) of 0.89, than **2**, with a (ϕ_Δ) of 0.66. The reason for this difference could be explained by the presence of an electron-rich dimethylamino group in **2**, which could cause intramolecular quenching by Photoinduced-Electron Transfer (PET) [51]. Notably, the absorption and emission spectra of **1** and **2** in phosphate-buffered saline (PBS, pH 7.4) are very broad (Fig. 3 and **Fig. S7**), indicative of aggregation, in agreement with the NMR, TEM and DLS studies. The broadening of the emission spectrum of **1** is notably larger than for **2**, confirming the higher tendency of the valine derivative to form colloidal species.

The generation of $^1O_2$ upon irradiation of **1** and **2** with white light (LED illumination in the range of 400–700 nm) was studied using two test reactions easily monitored by UV–Vis spectroscopy. The $^1O_2$ trap 9,10-dimethylanthracene (DMA) [19] and the analogous water-soluble trap 9,10-anthracenediyl-bis(methylene)-dimalonic acid (ABDA) [52] were employed. The former was used for acetonitrile and acetonitrile:PBS, and the latter for PBS (Fig. 4). In both cases, the decrease in the absorption band at 377 and 379 nm for DMA or ABDA, respectively, is a proof of reactivity towards $^1O_2$, since the reactions yield an endoperoxide not absorbing in that spectral region. The kinetics of the reaction were fitted to the pseudo-first-order model utilizing Eq. (1), where c is the concentration of probe molecule at certain time t (proportional to its absorbance, A), c_0 is the concentration of probe molecule at time 0, and k is the pseudo-first-order kinetic constant. This parameter is useful to compare the relative performance of the photosensitizers, although must not be taken as an absolute value to conclude about the reactivity of photosensitizers (solvent effects are very important).

$$ln\,(c/c_0) = ln\,(A/A_0) = -k{\cdot}t \quad (1)$$

The results of the irradiations can be seen in Fig. 4 in acetonitrile, acetonitrile:PBS and only PBS as media. The oxygenation reactions of

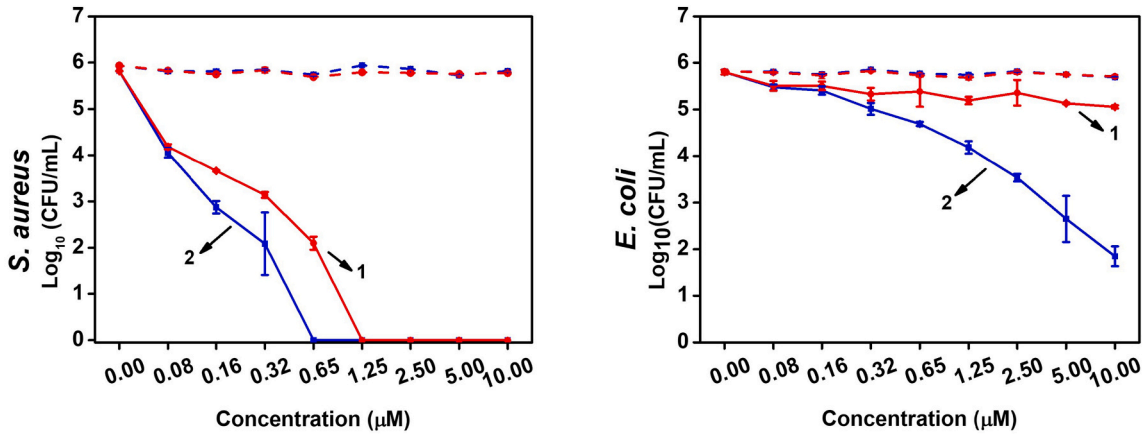

Fig. 5. Survival curves of *S. aureus* and *E. coli* (10^6 CFU/mL) incubated with different concentrations of **1** (red squares, continuous line) and **2** (blue squares, continuous line) and irradiated for 60 s. with a total energy dose of 5.3 J/cm^2 (LED white light, 400–700 nm). Control cells treated with **1** and **2** under dark conditions (red and blue circles, respectively) are also shown (dashed lines). (For interpretation of the references to colour in this figure legend, the reader is referred to the web version of this article.)

DMA in the cases of pure organic solvent occurred very rapidly, with almost complete bleaching in less than one minute, resulting in the following calculated constants: $k(\mathbf{1}) = 3.3$ min^{-1} and $k(\mathbf{2}) = 3.0$ min^{-1}. When using a mixed media of acetonitrile:PBS, the reactivity dropped almost to a half, with $k(\mathbf{1}) = 1.7$ min^{-1} and $k(\mathbf{2}) = 1.4$ min^{-1}. Finally, when PBS was used as the medium, the photooxygenation activity was completely stopped, with constants similar to the control irradiations without the presence of photosensitizer (ca. 0.004 min^{-1}). It must be noted that reactivity in an aqueous medium is slower than in organic solvents, due to the shorter lifetime of $^1O_2$, but this difference in lifetimes does not justify the absolute lack of absorption changes observed in the irradiated samples in PBS; the observed planarity of the kinetics in PBS would be indicative of the absence of $^1O_2$ generation. This result could be attributable to the already proven formation of aggregates (NMR, TEM, DLS) for both photosensitizers in such medium.

As already mentioned, the lack of $^1O_2$ generation in PBS was also described for phthalocyanine derivatives aggregated in the form of nanostructures, which did not impede their efficient antimicrobial photoactivity [32]. Encouraged by those findings, the photoantimicrobial action of **1** and **2** were tested with bacteria, specifically against a gram-positive species like *S. aureus* and a gram-negative species like *E. coli*. These bacteria are prototypic examples of "priority pathogens" identified by the WHO as major threats to human health [53]. In the first place, the uptake of **1** and **2** by these bacteria was demonstrated using Confocal Laser Scanning Microscopy (CLSM, **Fig. S11**) using the fluorescence of **1** and **2** as an indicator. Apparently, bacteria stained with **2** are marked with a higher brightness than bacteria treated with **1**. This could be because **2** bears a protonatable group and hence it must be in a cationic form in the aqueous media, and it is well known that the presence of cationic groups enhances the affinity of photosensitizers to the walls of bacteria [54].

Next, cultures of *S. aureus* and *E. coli* both with initial populations of approximately 10^6 cells/mL were incubated with different concentrations of **1** and **2** (from 0.08 to 10 μM) and irradiated with a total energy dose of 5.3 J/cm^2 (white light from a LED source, see details in the experimental section). The photodynamic effect was calculated using the plate-serial dilution spotting method (**Fig. S13**) [55,56]. Examining the survival curves shown in Fig. 5 it can be deduced that both photosensitizers had a dramatically different effect on both types of bacteria.

Both **1** and **2** reduce dramatically the population of *S. aureus,* whereas only **2** had some bactericidal action against *E. coli*. Examined in detail, the higher activity of **2** compared to **1**, must be ascribed to the aforementioned existence of a cationic group in the structure of **2**. Ammonium, pyridinium and phosphonium groups are paradigmatic examples that can be found in the literature which are capable of enhancing the binding to bacterial cell walls and consequently trigger a microbiocidal response [54]. This protonation does not occur in **1** and hence, this would explain why **2** is much more effective than **1** for both bacteria. As a matter of fact, it is well-known that the photoinactivation of gram-negative bacteria is especially inefficient by anionic and neutral photosensitizers, whereas cationic photosensitizers (like **2** in water) display reasonable activities (although typically less pronounced than against gram-positive bacteria) [10]. The higher activity against gram-positive *S. aureus* can be seen in the fact that total eradication of *S. aureus* (6 log CFU/mL reduction) occurred at concentrations of 1.25 μM for **1** and 0.65 μM for **2**, whereas neither **1** nor **2** was able to reduce such a significant population of the gram-negative bacteria. A significant parameter to estimate the antibacterial ability of a molecule under investigation is the concentration at which 99.9% (3 log CFU/mL) of the population of this bacteria is eliminated. According to the National Committee for Clinical Laboratory Standards, a chemical can be considered bactericidal when induces a reduction of population greater than 3 log CFU [57]. Hence, attending to this criterion and observing the results shown in Fig. 5, it must be concluded that **1** fulfils this requisite at 0.32 μM and **2** at 0.16 μM (for *S. aureus*). This later value is outstanding when compared to the data reported in the literature. Indeed, few reports describing photosensitizer with bactericidal capacities at the submicromolar concentration for gram-positive *S. aureus* have been described. For instance, a thiazine dye has been reported by Yao et al. at 0.5 μM [58]. Some examples of porphycenes also performed outstanding antibacterial outcomes. Hamblin and Nonell evaluated the antimicrobial photodynamic activity of a tri-cationic porphycene being bactericidal against *S. aureus* at 0.1 μM [59]. Hypericin is another example that is reported to trigger 3 log CFU/mL of reduction at 0.06 μM [60]. Furthermore, there have been a few studies concerning BODIPYs, particularly those cationic derivatives. Recently, Zhao et al. reported a pyridinium substituted BODIPY being bactericidal at 0.32 μM [43], which corroborates the potential of cationic BODIPYs already described by the O'Shea or Ghiladi groups just a few years before [37,38]. Durantini et al. and Piskorz et al. have also reported cationic BODIPYs being bactericidal at 0.5 μM [41,42].

For *E. coli*, although **1** did not show activity against this species, the minimal bactericidal activity of 3 log CFU employing **2** is observed at 2.5–5.0 μM (Fig. 5). These results were consistent with those from previous studies, confirming the higher difficulty for the elimination of gram-negative bacteria. For instance, a 5.0 μM concentration of photosensitizer is at least required for the cationic porphycenes reported by Hamblin and Nonell [59,61], and the thiazine dye reported by Yao was

Table 2
aPDI effect (log CFU /mL reduction) in the indicated microorganisms mediated by irradiation of photosensitizers (PS) **1** and **2**.

Compound	Bacteria	[PS] = 0.16 μM	[PS] = 0.65 μM	[PS] = 5.00 μM
1	*S. aureus*	2.3	3.9	6.0*
	E. coli	0.5	0.6	0.9
2	*S. aureus*	3.1	6.0*	6.0*
	E. coli	0.6	1.3	3.4

Asterisk (*) indicates total eradication.

found to be bactericidal at 6 μM [58]. A few BODIPYs have also been tested against *E.coli*. A dicationic aza-BODIPY described by O'Shea exhibited bactericidal capability at 4.3 μM [37]. More recently, Durantini et al. studied several cationic BODIPYs that induce a reduction of 3 logs at 5.0 μM [39]. Significantly better results have been achieved by Durantini in another study [41] or by Zhao et al. [43] utilizing BODIPY derivatives, being bactericidal at 1.0 μM and 1.25 μM, respectively. We have excluded from the above comparison the excellent results obtained by Nonell et al. using a combination of photosensitizer and gentamicin [62]. In Table 2, a summary of the photodynamic effects of **1** and **2** is compiled. Furthermore, to complete the study, the death of both *E. coli* and *S. aureus* was further confirmed by CLSM using the staining protocol with propidium iodide (**Fig. S14**) [63].

The bactericidal results here reported, confirm that despite the aggregation propensity of the photosensitizers in PBS, upon interaction with the microbial cell, the generation of cytotoxic $^1O_2$ is restored, probably because of disassembly. Thus, this finding supports the already proposed "one-for-all" strategy for the delivery of photo-drugs to kill microbial pathogens [32] but, in this case, using BODIPYs as photoactive scaffolds. Probably the described outstanding activity as antimicrobial photo-drug of **2** could be related to the fact that the bacterial cells (especially *S. aureus*) enter in contact with photosensitizer **2**, packed in the form of a nano-object, in other words, the local concentration of photosensitizer when the particle contacts with the wall must be considerably high. Being aware that many details are still missing in this preliminary model but given the potency of the antimicrobial action, this is a topic that deserves further investigation.

4. Conclusion

In summary, compounds **1** and **2** have been synthesized and characterized using $^1H/^{13}C$ NMR, HRMS, UV–Vis and fluorescence spectroscopies. Both compounds display the typical photophysical properties of bromo derivatives of BODIPY dyes in organic solvents (low ϕ_F and short τ_F along with high ϕ_Δ). In contrast, in aqueous media, the studied compounds tend to aggregate (NMR, UV–Vis, and fluorescence measurements) forming nano-objects of 370 nm (**1**) and 180 nm (**2**) diameter (as determined by DLS and TEM). The ability of **1** and **2** to generate efficiently $^1O_2$ in organic solvents has been demonstrated using DMA as a trap of this ROS. The generation of $^1O_2$ in the aqueous medium is stopped, probably because of the formation of aggregates. However, this apparent handicap is not an obstacle to the photo-antimicrobial activity, since when the aggregated photosensitizers are tested against *S. aureus* and *E. coli* (LED white light, using only 5.3 J/cm^2 energy dose), the minimal bactericidal activity of 3 logs CFU/mL is obtained at 2.5–5.0 μM for *E. coli* (employing **2**) and at submicromolar concentrations for *S. aureus* (0.31 μM for **1** and 0.16 μM for **2**).

CRediT authorship contribution statement

Diego Navarro-Barreda: Investigation. **Rosa de Llanos:** Investigation, Supervision, Conceptualization, Writing – review & editing. **Juan F. Miravet:** Conceptualization, Writing – review & editing. **Francisco Galindo:** Conceptualization, Supervision, Funding acquisition, Writing – review & editing.

Declaration of Competing Interest

The authors have no conflicts of interest to declare.

Acknowledgement

The authors acknowledge the financial support from the Spanish Ministry of Science and Innovation co-funded by the European Regional Development Fund of the European Union (grant RTI2018-101675-B-I00), Universitat Jaume I (grant UJI-B2021-51 and grant UJI-A2020-15). RdL was funded through a Beatriz Galindo Fellowship of the Ministerio de Educación y Formación Profesional, Spanish Government (BGP18/00062). SCIC from UJI is acknowledged for technical assistance.

Appendix A. Supplementary data

Supplementary data to this article can be found online at https://doi.org/10.1016/j.jphotobiol.2022.112543.

References

[1] C. Nathan, Resisting antimicrobial resistance, Nat. Rev. Microbiol. 18 (2020) 259–260, https://doi.org/10.1038/s41579-020-0348-5.
[2] P. Beyer, S. Paulin, The antibacterial research and development pipeline needs urgent solutions, ACS Infect. Dis. 6 (2020) 1289–1291, https://doi.org/10.1021/acsinfecdis.0c00044.
[3] S. Nonell, C. Flors (Eds.), Singlet Oxygen: Applications in Biosciences and Nanosciences Vol. 1, The Royal Society of Chemistry, 2016, https://doi.org/10.1039/9781782622208.
[4] M. Wainwright, Anti-infective dyes in the time of COVID, Dyes Pigments 196 (2021), 109813, https://doi.org/10.1016/j.dyepig.2021.109813.
[5] M.R. Hamblin, T. Hasan, Photodynamic therapy: a new antimicrobial approach to infectious disease? Photochem. Photobiol. Sci. 3 (2004) 436–450, https://doi.org/10.1039/b311900a.
[6] T. Maisch, R.M. Szeimies, G. Jori, C. Abels, Antibacterial photodynamic therapy in dermatology, Photochem. Photobiol. Sci. 3 (2004) 907–917, https://doi.org/10.1039/b407622b.
[7] D.A. Phoenix, S.R. Dennison, F. Harris, Photodynamic antimicrobial chemotherapy, Nov. Antimicrob. Agents Strateg. (2014) 295–330, https://doi.org/10.1002/9783527676132.ch10.
[8] E. Alves, M.A.F. Faustino, M.G.P.M.S. Neves, Â. Cunha, H. Nadais, A. Almeida, Potential applications of porphyrins in photodynamic inactivation beyond the medical scope, J. Photochem. Photobiol. C Photochem. Rev. 22 (2015) 34–57, https://doi.org/10.1016/j.jphotochemrev.2014.09.003.
[9] M.R. Hamblin, Antimicrobial photodynamic inactivation: a bright new technique to kill resistant microbes, Curr. Opin. Microbiol. 33 (2016) 67–73, https://doi.org/10.1016/j.mib.2016.06.008.
[10] M. Wainwright, T. Maisch, S. Nonell, K. Plaetzer, A. Almeida, G.P. Tegos, M. R. Hamblin, Photoantimicrobials—are we afraid of the light? Lancet Infect. Dis. 17 (2017) e49–e55, https://doi.org/10.1016/S1473-3099(16)30268-7.
[11] F. Cieplik, D. Deng, W. Crielaard, W. Buchalla, E. Hellwig, A. Al-Ahmad, T. Maisch, Antimicrobial photodynamic therapy–what we know and what we don't, Crit. Rev. Microbiol. 44 (2018) 571–589, https://doi.org/10.1080/1040841X.2018.1467876.
[12] V. Pérez-Laguna, Y. Gilaberte, M.I. Millán-Lou, M. Agut, S. Nonell, A. Rezusta, M. R. Hamblin, A combination of photodynamic therapy and antimicrobial compounds to treat skin and mucosal infections: a systematic review, Photochem. Photobiol. Sci. 18 (2019) 1020–1029, https://doi.org/10.1039/c8pp00534f.
[13] A. Anas, J. Sobhanan, K.M. Sulfiya, C. Jasmin, P.K. Sreelakshmi, V. Biju, Advances in photodynamic antimicrobial chemotherapy, J. Photochem. Photobiol. C Photochem. Rev. 49 (2021), 100452, https://doi.org/10.1016/j.jphotochemrev.2021.100452.
[14] D.A. Heredia, A.M. Durantini, J.E. Durantini, E.N. Durantini, Fullerene C60 derivatives as antimicrobial photodynamic agents, J. Photochem. Photobiol. C Photochem. Rev. 51 (2022), https://doi.org/10.1016/j.jphotochemrev.2021.100471.
[15] H. Abrahamse, M.R. Hamblin, New photosensitizers for photodynamic therapy, Biochem. J. 473 (2016) 347–364, https://doi.org/10.1042/BJ20150942.
[16] B. Ran, Z. Wang, W. Cai, L. Ran, W. Xia, W. Liu, X. Peng, Organic photo-antimicrobials: principles, molecule design, and applications, J. Am. Chem. Soc. 143 (2021) 17891–17909, https://doi.org/10.1021/jacs.1c08679.
[17] C. Spagnul, L.C. Turner, R.W. Boyle, Immobilized photosensitizers for antimicrobial applications, J. Photochem. Photobiol. B Biol. 150 (2015) 11–30, https://doi.org/10.1016/j.jphotobiol.2015.04.021.
[18] A. Beltrán, M. Mikhailov, M.N. Sokolov, V. Pérez-Laguna, A. Rezusta, M.J. Revillo, F. Galindo, A photobleaching resistant polymer supported hexanuclear molybdenum iodide cluster for photocatalytic oxygenations and photodynamic

inactivation of: *Staphylococcus aureus*, J. Mater. Chem. B 4 (2016) 5975–5979, https://doi.org/10.1039/c6tb01966h.
[19] C. Felip-León, C. Arnau Del Valle, V. Pérez-Laguna, M. Isabel Millán-Lou, J. F. Miravet, M. Mikhailov, M.N. Sokolov, A. Rezusta-López, F. Galindo, Superior performance of macroporous over gel type polystyrene as a support for the development of photo-bactericidal materials, J. Mater. Chem. B 5 (2017) 6058–6064, https://doi.org/10.1039/c7tb01478c.
[20] C.A. del Valle, V. Pérez-Laguna, I.M. Resta, R. Gavara, C. Felip-León, J.F. Miravet, A. Rezusta, F. Galindo, A cost-effective combination of rose Bengal and off-the-shelf cationic polystyrene for the photodynamic inactivation of *Pseudomonas aeruginosa*, Mater. Sci. Eng. C. 117 (2020), 111302, https://doi.org/10.1016/j.msec.2020.111302.
[21] N. López-López, I. Muñoz Resta, R. De Llanos, J.F. Miravet, M. Mikhaylov, M. N. Sokolov, S. Ballesta, I. García-Luque, F. Galindo, Photodynamic inactivation of *Staphylococcus aureus* biofilms using a Hexanuclear molybdenum complex embedded in transparent polyHEMA hydrogels, ACS biomater, Sci. Eng. 6 (2020) 6995–7003, https://doi.org/10.1021/acsbiomaterials.0c00992.
[22] R. Gavara, R. de Llanos, V. Pérez-Laguna, C. Arnau del Valle, J.F. Miravet, A. Rezusta, F. Galindo, Broad-Spectrum photo-antimicrobial polymers based on cationic polystyrene and rose Bengal, Front. Med. 8 (2021) 1–10, https://doi.org/10.3389/fmed.2021.641646.
[23] A.M. López-Fernández, I. Muñoz Resta, R. De Llanos, F. Galindo, Photodynamic inactivation of *Pseudomonas aeruginosa* by PHEMA films loaded with rose Bengal: potentiation effect of potassium iodide, Polymers (Basel). 13 (2021), https://doi.org/10.3390/polym13142227.
[24] M. Bregnhøj, M. Westberg, F. Jensen, P.R. Ogilby, Solvent-dependent singlet oxygen lifetimes: temperature effects implicate tunneling and charge-transfer interactions, Phys. Chem. Chem. Phys. 18 (2016) 22946–22961, https://doi.org/10.1039/c6cp01635a.
[25] A. Bekmukhametova, H. Ruprai, J.M. Hook, D. Mawad, J. Houang, A. Lauto, Photodynamic therapy with nanoparticles to combat microbial infection and resistance, Nanoscale. 12 (2020) 21034–21059, https://doi.org/10.1039/d0nr04540c.
[26] E. Anaya-Plaza, E. van de Winckel, J. Mikkilä, J.M. Malho, O. Ikkala, O. Gulías, R. Bresolí-Obach, M. Agut, S. Nonell, T. Torres, M.A. Kostiainen, A. de la Escosura, Photoantimicrobial biohybrids by supramolecular immobilization of cationic Phthalocyanines onto cellulose nanocrystals, Chem. - A Eur. J. 23 (2017) 4320–4326, https://doi.org/10.1002/chem.201605285.
[27] A. Galstyan, A. Ricker, H. Nüsse, J. Klingauf, U. Dobrindt, Exploring the impact of coordination-driven self assembly on the antibacterial activity of low-symmetry Phthalocyanines, ACS Appl. Bio Mater. 3 (2020) 400–411, https://doi.org/10.1021/acsabm.9b00873.
[28] M.Á. Revuelta-Maza, E. De Las Heras, M. Agut, S. Nonell, T. Torres, G. De La Torre, Self-assembled Binaphthyl-bridged amphiphilic AABB Phthalocyanines: nanostructures for efficient antimicrobial photodynamic therapy, Chem. - A Eur. J. 27 (2021) 4955–4963, https://doi.org/10.1002/chem.202005060.
[29] X. Li, S. Yu, Y. Lee, T. Guo, N. Kwon, D. Lee, S.C. Yeom, Y. Cho, G. Kim, J.D. Huang, S. Choi, K.T. Nam, J. Yoon, In vivo albumin traps photosensitizer monomers from self-assembled phthalocyanine nanovesicles: a facile and switchable theranostic approach, J. Am. Chem. Soc. 141 (2019) 1366–1372, https://doi.org/10.1021/jacs.8b12167.
[30] Y.Y. Zhao, L. Zhang, Z. Chen, B.Y. Zheng, M. Ke, X. Li, J.D. Huang, Nanostructured phthalocyanine assemblies with efficient synergistic effect of type i photoreaction and Photothermal action to overcome tumor hypoxia in photodynamic therapy, J. Am. Chem. Soc. 143 (2021) 13980–13989, https://doi.org/10.1021/jacs.1c07479.
[31] N.M. Casellas, G. Dai, E.Y. Xue, A. Fonseca, D.K.P. Ng, M. García-Iglesias, T. Torres, A self-assembled subphthalocyanine-based nanophotosensitiser for photodynamic therapy, Chem. Commun. 58 (2022) 669–672, https://doi.org/10.1039/d1cc05977g.
[32] I. Paramio, T. Torres, G. de la Torre, Self-assembled Porphyrinoids: one-component nanostructured Photomedicines, ChemMedChem. 16 (2021) 2441–2451, https://doi.org/10.1002/cmdc.202100201.
[33] A. Kamkaew, S.H. Lim, H.B. Lee, L.V. Kiew, L.Y. Chung, K. Burgess, BODIPY dyes in photodynamic therapy, Chem. Soc. Rev. 42 (2013) 77–88, https://doi.org/10.1039/c2cs35216h.
[34] A.M. Durantini, D.A. Heredia, J.E. Durantini, E.N. Durantini, BODIPYs to the rescue: potential applications in photodynamic inactivation, Eur. J. Med. Chem. 144 (2018) 651–661, https://doi.org/10.1016/j.ejmech.2017.12.068.
[35] M.L. Agazzi, M.B. Ballatore, A.M. Durantini, E.N. Durantini, A.C. Tomé, BODIPYs in antitumoral and antimicrobial photodynamic therapy: an integrating review, J. Photochem. Photobiol. C Photochem. Rev. 40 (2019) 21–48, https://doi.org/10.1016/j.jphotochemrev.2019.04.001.
[36] R. Prieto-Montero, A. Prieto-Castañeda, R. Sola-Llano, A.R. Agarrabeitia, D. García-Fresnadillo, I. López-Arbeloa, A. Villanueva, M.J. Ortiz, S. de la Moya, V. Martínez-Martínez, Exploring BODIPY derivatives as singlet oxygen photosensitizers for PDT, Photochem. Photobiol. 96 (2020) 458–477, https://doi.org/10.1111/php.13232.
[37] D.O. Frimannsson, M. Grossi, J. Murtagh, F. Paradisi, D.F. Oshea, Light induced antimicrobial properties of a brominated boron difluoride (BF2) chelated tetraarylazadipyrromethene photosensitizer, J. Med. Chem. 53 (2010) 7337–7343, https://doi.org/10.1021/jm100585j.
[38] B.L. Carpenter, X. Situ, F. Scholle, J. Bartelmess, W.W. Weare, R.A. Ghiladi, Antiviral, antifungal and antibacterial activities of a BODIPY-based photosensitizer, Molecules. 20 (2015) 10604–10621, https://doi.org/10.3390/molecules200610604.
[39] M.L. Agazzi, M.B. Ballatore, E. Reynoso, E.D. Quiroga, E.N. Durantini, Synthesis, spectroscopic properties and photodynamic activity of two cationic BODIPY derivatives with application in the photoinactivation of microorganisms, Eur. J. Med. Chem. 126 (2017) 110–121, https://doi.org/10.1016/j.ejmech.2016.10.001.
[40] K. Gu, G. Lin, Y. Zhu, X. Ji, J. Li, X. Dong, W. Zhao, Anchoring BODIPY photosensitizers enable pan-microbial photoinactivation, Eur. J. Med. Chem. 199 (2020), 112361, https://doi.org/10.1016/j.ejmech.2020.112361.
[41] Y.B. Palacios, S.C. Santamarina, J.E. Durantini, E.N. Durantini, A.M. Durantini, BODIPYs bearing a dimethylaminopropoxy substituent for imaging and photodynamic inactivation of bacteria, J. Photochem. Photobiol. B Biol. 212 (2020), 112049, https://doi.org/10.1016/j.jphotobiol.2020.112049.
[42] J. Piskorz, W. Porolnik, M. Kucinska, J. Dlugaszewska, M. Murias, J. Mielcarek, BODIPY-based photosensitizers as potential anticancer and antibacterial agents: role of the positive charge and the heavy atom effect, ChemMedChem. 16 (2021) 399–411, https://doi.org/10.1002/cmdc.202000529.
[43] G. Lin, M. Hu, R. Zhang, Y. Zhu, K. Gu, J. Bai, J. Li, X. Dong, W. Zhao, Discovery of Meso-(meta-Pyridinium) BODIPY photosensitizers: in vitro and in vivo evaluations for antimicrobial photodynamic therapy, J. Med. Chem. 64 (2021) 18143–18157, https://doi.org/10.1021/acs.jmedchem.1c01643.
[44] M.J. Ortiz, A.R. Agarrabeitia, G. Duran-Sampedro, J. Bañuelos Prieto, T.A. Lopez, W.A. Massad, H.A. Montejano, N.A. García, I. Lopez Arbeloa, Synthesis and functionalization of new polyhalogenated BODIPY dyes. Study of their photophysical properties and singlet oxygen generation, Tetrahedron. 68 (2012) 1153–1162, https://doi.org/10.1016/j.tet.2011.11.070.
[45] C.A. Angulo-Pachón, D. Navarro-Barreda, C.M. Rueda, F. Galindo, J.F. Miravet, Deamidation of pseudopeptidic molecular hydrogelators and its application to controlled release, J. Colloid Interface Sci. 505 (2017) 1111–1117, https://doi.org/10.1016/j.jcis.2017.07.003.
[46] D. Navarro-Barreda, C.A. Angulo-Pachón, B. Bedrina, F. Galindo, J.F. Miravet, A dual stimuli responsive supramolecular gel provides insulin hydrolysis protection and redox-controlled release of actives, Macromol. Chem. Phys. 221 (2020) 1900419, https://doi.org/10.1002/macp.201900419.
[47] D. Navarro-Barreda, C.A. Angulo-Pachón, F. Galindo, J.F. Miravet, Photoreversible formation of nanotubes in water from an amphiphilic azobenzene derivative, Chem. Commun. 57 (2021) 11545–11548, https://doi.org/10.1039/d1cc04319f.
[48] D. Navarro-Barreda, B. Bedrina, F. Galindo, J.F. Miravet, Glutathione-responsive molecular nanoparticles from a dianionic bolaamphiphile and their use as carriers for targeted delivery, J. Colloid Interface Sci. 608 (2022) 2009–2017, https://doi.org/10.1016/j.jcis.2021.10.142.
[49] D. Navarro-Barreda, B. Bedrina, C.A. Angulo-Pachón, J.F. Miravet, D. Pérez-Sala, F. Galindo, Structure-performance relationships of four lysosomal markers used for the imaging of HT-29 cancer cells and a cellular model of lysosomal storage disease (Niemann-Pick C), Dyes Pigments 201 (2022), 110236, https://doi.org/10.1016/j.dyepig.2022.110236.
[50] B. Escuder, M.L. Lusar, J.F. Miravet, Insight on the NMR study of supramolecular gels and its application to monitor molecular recognition on self-assembled fibers, J. Org. Chem. 71 (2006) 7747–7752, https://doi.org/10.1021/jo0612731.
[51] F. Galindo, M.I. Burguete, L. Vigara, S.V. Luis, N. Kabir, J. Gavrilovic, D.A. Russell, Synthetic macrocyclic peptidomimetics as tunable pH probes for the fluorescence imaging of acidic organelles in Live cells, Angew. Chemie Int. Ed. 44 (2005) 6504–6508, https://doi.org/10.1002/anie.200501920.
[52] C. Felip-León, M. Puche, J.F. Miravet, F. Galindo, M. Feliz, A spectroscopic study to assess the photogeneration of singlet oxygen by graphene oxide, Mater. Lett. 251 (2019) 45–51, https://doi.org/10.1016/j.matlet.2019.05.001.
[53] U. Theuretzbacher, K. Bush, S. Harbarth, M. Paul, J.H. Rex, E. Tacconelli, G. E. Thwaites, Critical analysis of antibacterial agents in clinical development, Nat. Rev. Microbiol. 18 (2020) 286–298, https://doi.org/10.1038/s41579-020-0340-0.
[54] M.C. Jennings, K.P.C. Minbiole, W.M. Wuest, Quaternary ammonium compounds: an antimicrobial mainstay and platform for innovation to address bacterial resistance, ACS Infect. Dis. 1 (2016) 288–303, https://doi.org/10.1021/acsinfecdis.5b00047.
[55] S. Sieuwerts, F.A.M. De Bok, E. Mols, W.M. De Vos, J.E.T. Van Hylckama Vlieg, A simple and fast method for determining colony forming units, Lett. Appl. Microbiol. 47 (2008) 275–278, https://doi.org/10.1111/j.1472-765X.2008.02417.x.
[56] H. Naghili, H. Tajik, K. Mardani, S.M. Razavi Rouhani, A. Ehsani, P. Zare, Validation of drop plate technique for bacterial enumeration by parametric and nonparametric tests, Vet. Res. Forum an Int. Q. J. 4 (2013) 179–183. http://www.ncbi.nlm.nih.gov/pubmed/25653794%0Ahttp://www.pubmedcentral.nih.gov/articlerender.fcgi?artid=PMC4312378.
[57] R.D. Pearson, R.T. Steigbigel, H.T. Davis, S.W. Chapman, Method for reliable determination of minimal lethal antibiotic concentrations, Antimicrob. Agents Chemother. 18 (1980) 699–708, https://doi.org/10.1128/AAC.18.5.699.
[58] Q. Xiao, B. Mai, Y. Nie, C. Yuan, M. Xiang, Z. Shi, J. Wu, W. Leung, C. Xu, S.Q. Yao, P. Wang, L. Gao, In vitro and in vivo demonstration of ultraefficient and broad-spectrum antibacterial agents for photodynamic antibacterial chemotherapy, ACS Appl. Mater. Interfaces 13 (2021) 11588–11596, https://doi.org/10.1021/acsami.0c20837.
[59] X. Ragàs, D. Sánchez-García, R. Ruiz-González, T. Dai, M. Agut, M.R. Hamblin, S. Nonell, Cationic porphycenes as potential photosensitizers for antimicrobial photodynamic therapy, J. Med. Chem. 53 (2010) 7796–7803, https://doi.org/10.1021/jm1009555.
[60] I. García, S. Ballesta, Y. Gilaberte, A. Rezusta, Á. Pascual, Antimicrobial photodynamic activity of hypericin against methicillin-susceptible and resistant *Staphylococcus aureus* biofilms, Future Microbiol. 10 (2015) 347–356, https://doi.org/10.2217/FMB.14.114.

[61] R. Ruiz-González, M. Agut, E. Reddi, S. Nonell, A comparative study on two cationic porphycenes: Photophysical and antimicrobial photoinactivation evaluation, Int. J. Mol. Sci. 16 (2015) 27072–27086, https://doi.org/10.3390/ijms161125999.

[62] I. Nieves, C. Hally, C. Viappiani, M. Agut, S. Nonell, A porphycene-gentamicin conjugate for enhanced photodynamic inactivation of bacteria, Bioorg. Chem. 97 (2020), 103661, https://doi.org/10.1016/j.bioorg.2020.103661.

[63] L. Boulos, M. Prévost, B. Barbeau, J. Coallier, R. Desjardins, LIVE/DEAD(®) BacLight(TM): application of a new rapid staining method for direct enumeration of viable and total bacteria in drinking water, J. Microbiol. Methods 37 (1999) 77–86, https://doi.org/10.1016/S0167-7012(99)00048-2.